Soft Matter

ROYAL SOCIETY OF CHEMISTRY

PAPER

View Article Online
View Journal | View Issue

Check for updates

Cite this: *Soft Matter*, 2025, **21**, 4434

Young's modulus of multinanolayer polymer films: the role of the interfaces†

Alvaro A. Grandi,*[a] Alain Guinault,[a] Jorge Peixinho,[a] Cyrille Sollogoub,[a] Arnaud Antkowiak,[b] Sébastien Neukirch[b] and Guillaume Miquelard-Garnier*[a]

Received 18th February 2025,
Accepted 5th May 2025

DOI: 10.1039/d5sm00175g

rsc.li/soft-matter-journal

The number of free surfaces in a polymer ultra-thin film has a strong influence on its physical and mechanical properties. In this study, Young's modulus as well as the glass transition temperature of multinanolayer coextruded polymer films, hence with no free surfaces, have been measured. We observe that contrary to the case of freestanding or supported ultra-thin films, there is no depression of the glass transition temperature or the Young modulus, but an increase for the latter as the layer thickness decreases, whatever the polymer pair (with various compatibilities). It is proposed that this increase is associated with the rise of interphase volume fraction in the films. An interphase modulus of about 25 GPa can be extracted from the empirical model, about 10 times higher than the typical modulus value of a glassy polymer. This value does not appear to depend on the nature of the polymers, meaning that the presence of entanglements at the interfaces is not a key factor to explain the increase in Young's modulus of multinanolayer films.

1 Introduction

Thin polymer films can find applications in numerous industrial fields, from organic electronics[1,2] to food packaging.[3,4] However, for ultra-thin films, *i.e.* when the thickness becomes similar to the typical macromolecular dimension (∼50 nm), it has been observed that several physical properties can decrease with decreasing thickness, reaching values significantly lower than those of the bulk.[5,6] For example, the depletion of the polystyrene (PS) glass transition temperature has been thoroughly characterized,[5,7,8] as well as its viscosity.[9] This loss has also been observed, again on PS ultra-thin films, for several mechanical properties such as maximum stress,[10] toughness,[10] fracture strength[11] and Young's modulus.[12,13]

The origin of this drop in physical properties has long been debated: as the preparation and measurement of such films is complicated, several authors suggested it could be an experimental artifact due to measurement method or sample preparation,[14] or on the contrary intrinsic and due to confinement and the presence of free surfaces.[15] Concerning the drop in glass transition temperature, there is now a reasonable consensus linking it to the presence of free surfaces,[16] regardless of geometry.[17] Free surfaces lead to enhanced surface mobility, resulting in the existence of a thin layer (∼1 nm) of liquid-like material at the free surface.[9,18] A "global" glass transition temperature T_g for the ultra-thin film lower than the bulk one is then observed. Comforting this hypothesis, the cases of supported (resting on a substrate)[16] or gold-capped[19] PS ultra-thin films show no T_g variation, while other polymers such as poly(methyl methacrylate) (PMMA) may even display an increase in T_g due to specific interactions (H-bonds) with silica substrates.[20] More recently, the role of polymer–polymer interfaces on the local dynamics in ultra-thin films has also attracted attention: although enhanced diffusion dynamics was measured for confined PS near a PMMA interface by Koo *et al.*,[21] an increase in T_g has been characterized for PS near polysulfone (PSF) or PMMA (hard confinement), while a decrease was observed near poly(isobutyl methacrylate) (PiBMA) (soft confinement).[22,23]

Concerning mechanical properties, the reduction has been linked to the same increase in molecular mobility in the layer near the free surface, but also to the reduction of entanglements due to confinement.[24–26] Recently, the group of Crosby has proposed a semi-empirical model derived from Mikos and Peppas approach that links entanglements to strength and toughness of polymer glasses,[27] adapted to ultra-thin films.[10] The model specifically aims at decoupling entanglements from mobility effects to account for the drop in strength.

---

[a] *Laboratoire PIMM, CNRS, Arts et Métiers Institute of Technology, Cnam, 151 Boulevard de l'Hôpital, Paris 75013, France. E-mail: alvaro.anzoleaga_grandi@ensam.eu, guillaume.miquelardgarnier@lecnam.net*

[b] *Institut Jean Le Rond d'Alembert, CNRS, Sorbonne Université, F-75005 Paris, France*

† Electronic supplementary information (ESI) available. See DOI: **https://doi.org/10.1039/d5sm00175g**

Multinanolayer coextrusion is an innovative process to produce extruded films made of two (or more) polymers, where the number of layers within the film (hence the number of interfaces) and their thickness can be controlled separately.[28–30] In multinanolayered films made of thousands of alternating layers, the layer thickness becomes also comparable to the typical size of the macromolecules, which can result in a significant improvement in various properties,[31,32] *e.g.* gas barrier or birefringence. Moreover, the thousands of interfaces lead to a considerable increase in the volume fraction of interfaces in the materials.[33] These samples can then be characterized with classical polymer analysis techniques to probe the role of the interfaces on the final properties, and even measure quantitatively the interfacial properties. Recently, we have shown for example that the rheological properties of compatibilized as well as non-compatibilized interphases of immiscible polymer blends can be obtained from such samples using a conventional rheometer.[33,34] Notably, significantly higher properties were obtained for the interphase compared to the bulk properties, with the appearance of an interphase modulus at high strain rates in the case of non-compatibilized nanolayered PS–PMMA films.[34]

This work aims at extending this approach to the solid state to measure mechanical properties, and especially the Young modulus. The focus here is double: first, surface effect on the modulus will be assessed by comparing nanolayered films having two polymer–polymer interfaces (hence no free surfaces) with literature results on supported (on a solid or liquid substrate[26,35]) and freestanding ultra-thin films (as depicted in Fig. 1), similar to what has been done on the dewetting of such films.[36,37] Second, the effect of the interfacial thickness will be discussed, by comparing three immiscible polymer pairs with different compatibilities, as it has been for example quantitatively related to other mechanical properties such as interfacial adhesion.[38–40]

2 Experimental

2.1 Materials

Multinanolayer coextruded films were fabricated using a lab-made coextrusion line described previously in details.[34,42,43] Briefly, two 20 mm single-screw extruders are fed with the chosen polymer pair. After a feedblock generating a trilayer flow, a series of layer-multiplying elements (LME) split it vertically, spread it horizontally, and then recombine it. Passing through N LMEs results in a film with $n_{\text{tot}} = 2^{N+1} + 1$ total layers. This method allows film production with a total thickness H on the order of 100 μm, with thousands of alternating layers of the two polymers, with thicknesses down to $h \sim 50$ nm. For the inner polymer, the layer thickness is deduced as:

$$h = H\frac{\phi}{2^N} \tag{1}$$

with ϕ its volume fraction.

Previous studies[41,44] have shown that for a given film the mean experimental layer thickness and the value obtained from eqn (1) were in quantitative agreement, so the latter will systematically be used in the following. As a first approach the distribution of layer thicknesses around the mean value will not be considered. Note that what is called here a layer typically corresponds, in terms of thickness, to what is designed under the name of ''ultra-thin film'' when dealing with a single-layer film (see Fig. 1). In the following, nanolayers (from multinanolayer films) will then be compared to free-standing and supported ultra-thin films.

In this study, three different set of coextruded polymer films have been used. The main properties of the neat polymers are listed in Table 1.

The first set is made of PS 1340 from Total and PMMA VM100 from Arkema with a PS/PMMA weight composition close to 60/40 wt%. PS and PMMA are two glassy polymers with similar glass transition temperatures, T_g, as shown in Table 1. The detailed fabrication process and rheology study of these coextruded films is presented in the works of Dmochowska *et al.*[34,48] Films with 3, 17, 129, 2049 and 4097 layers were prepared. The films were collected using a chill roll with the lowest possible drawing speed to prevent as much as possible chain extension in the extrusion direction. To reduce the thickness of the final film (hence of the individual layers) without a significant post-stretching step, a sacrificial layer of low density polyethylene (LDPE 1022 FN, TotalEnergies) was added at the exit die. The layer thicknesses within the prepared films range from ∼100 μm to 80 nm. The second coextruded films are made of polycarbonate (PC) and styrene-acrylonitrile (SAN) both from Trinseo with a PC/SAN weight composition close to 80/20 wt% (see ref. 47 for a detailed explanation of the fabrication process). In this case, the two glassy polymers have

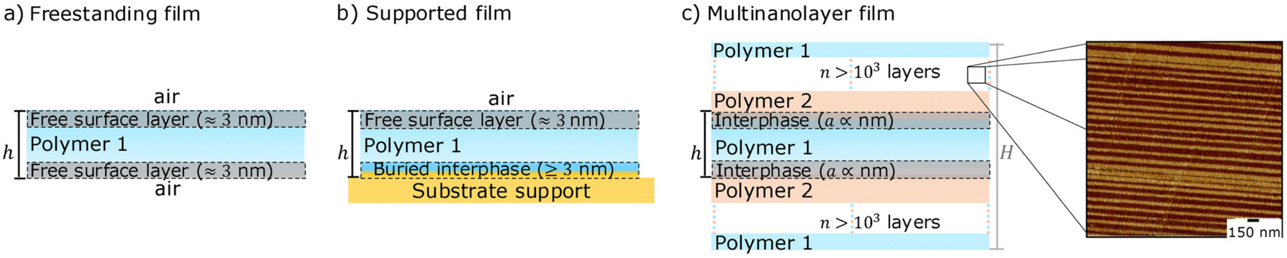

Fig. 1 Different types of ultra-thin polymer layers, depending on the number of free surfaces. (a) Freestanding: two free surfaces. (b) Supported (deposited on a surface): one free surface. (c) Multinanolayer coextruded films where the internal layers have no free surface, but polymer–polymer interphases with the adjacent layers. On the right, a typical AFM image of a portion of a coextruded multinanolayer film (here, PS/PMMA).[41]

Table 1 Physical properties of the constituent polymers

Neat polymer	T_g (°C)	M_w (kg mol^{-1})	R_{ee} (nm)	Coextruded with
PS	104	245	26[45]	PMMA
PMMA	99	139	20[45]	PS
PC	138	62	16[46]	SAN
SAN	94	95	17[46,47]	PC
PA6	60	124	13[33,45]	PE
PE	∼−100	122	12[33,45]	PA6

significantly different T_g (see Table 1). Films with 17, 65, 129, 513, 1025 and 2049 layers were produced, with layer thicknesses ranging from ∼10 μm to 50 nm. The last set of films is made of polyethylene (PE), polyethylene-*graft*-maleic anhydride (PEgMA) as a compatibilizer both from Dow Chemical Company and polyamide 6 (PA6) from BASF with a PE/PEgMA/PA weight composition of 25/50/25 wt%. Both PE and PA6 are semi-crystalline polymers, one with T_g well below room temperature (RT), the other above RT (see Table 1). Films with 3, 129 and 2049 layers were used in this study, with layer thicknesses ranging again from ∼10 μm to 50 nm. The detailed experimental set-up and fabrication process can be found in ref. 33 and 49. For all multinanolayer films selected in this study, processing conditions were such that the amount of ruptured layers was negligible ($\lesssim$5%), so the layers will be considered continuous with uniform thickness in the following.

These three set of polymer pairs (PS/PMMA, PC/SAN and PE/PA) can be compared in terms of compatibility, which will affect the thickness of the interfacial region, *i.e.* the interphase (Fig. 1c). At thermodynamic equilibrium, the interphase thickness can be defined as $a \approx 2b/\sqrt{6\chi}$[50] where χ is the Flory–Huggins interaction parameter and b is the effective length per monomer unit. For the polymer pairs of the present study, the values are: $a_{\mathrm{PS/PMMA}} \approx 3$ nm[34,51,52] and $a_{\mathrm{PC/SAN}} \approx 7$ nm.[46] In the PE/PA system, due to the *in situ* formation of a compatibilizing copolymer segregating at the interfaces, the interphase thickness can be considered as the end-to-end distance of this copolymer, as discussed in Beuguel *et al.*,[33] so $a_{\mathrm{PE/PA}} \approx 30$ nm.

2.2 Methods

Dynamic mechanical analysis (DMA) was performed to obtain T_g for the neat polymers (Table 1) and for the fabricated multinanolayer films. The thermomechanical properties were characterized in tension mode with a Q800 apparatus (TA Instruments). For the PS/PMMA multinanolayer films, the temperature scan was performed from 35 up to 180 °C. For the PC/SAN multinanolayer films the temperature scan was performed from 40 up to 160 °C. In both cases, the heating rate was 2 °C min^{-1}, the frequency 1 Hz and the strain 0.1%, within the linear regime.

A three-point bending test has been designed using a Deben microtest machine to measure Young's modulus E. This mechanical test has been chosen over more classical tensile tests because it has a motion perpendicular to the extrusion direction, allowing mechanical solicitation of the multiple interfaces.[53] The tests were performed at RT, with displacement applied at a constant velocity of 1.5 mm s^{-1}. The samples were cut from the middle of the extruded film parallel to the extrusion flow to obtain the desired geometry, *i.e.* a constant width w and length l of 1 cm and 5 cm, respectively (see Fig. S1a in the ESI†). The thickness of the sample is measured five times across the entire width using a contact profilometer to obtain an accurate average of the total thickness H. Then the thickness h of the inner polymer is deduced from eqn (1) for each sample. It has been verified in previous studies[33,34] with AFM measurements that the obtained value is consistent with the layers' experimental thickness.[44] To capture the displacement y, the setup is placed under a routine stereo microscope Leica M80 and an image is recorded every 0.5 mm. The system is seen as a simply supported beam (see Fig. S1b in ESI†) with a central load following the Euler–Bernoulli beam theory.[54,55] In this case, Young's modulus of the coextruded film can be deduced from the equation:

$$E = \frac{FL^3}{4wyH^3} \tag{2}$$

with F the measured force and y the displacement of the center of the beam.

Fig. S1c (see the ESI†) shows that for the studied samples, we can consider there is no slip between the layers during the test, confirming the use of eqn (2) for Young's modulus.

In the case of thinner films, the bending force was sometimes too low and its measurement not accurate enough. In this situation, several films were stacked and thermo-pressed together. It was verified on thicker films that this additional preparation step does not change the values obtained for the modulus (see Fig. S2a in ESI†).

When bending is applied on unidirectional films with continuous layers, and parallel to their extruded direction, a simple estimate of Young's modulus of the film can be obtained from the simple rule of mixtures[56,57] $E_{\mathrm{film}} = \sum_i \phi_i E_i$, where ϕ_i is the volume fraction and E_i the Young modulus of the neat polymers. In the case of two components, the equation can be simply written as $E_{\mathrm{film}} = \phi E_1 + (1 - \phi)E_2$. The mixing rule value can then be compared with the experimental data, with a quantitative agreement if confinement and/or interfacial effects are negligible.

3 Results and discussion

As mentioned previously, Bay *et al.*[10] recently proposed a semi-empirical model taking into account the effect of entanglements and chain mobility to explain the decrease in maximum stress and toughness in ultra-thin films of glassy polymers. Adapting their model for Young's modulus, it can be written as follows:

$$E(h, M_w) = \alpha\left(T - T_g(h)\right) + \beta \exp\left(\frac{-2}{\langle M_w/M_e(h)\rangle}\right) \tag{3}$$

where T is the temperature of the test, $T_g(h)$ is the glass transition temperature depending on the thickness h of the ultra-thin film, and (α, β) are two empirical parameters. The ratio of the weight average molecular weight M_w to the entanglement molecular weight $M_e(h)$ characterizes the level of entanglements.[27] Fig. S3 in ESI,† confirms the good agreement between this model and experimental data from the literature on polymers with one and two free surfaces.

In the case of the multinanolayer films studied here, the average end-to-end distance of the polymer chain, R_{ee}, has been determined using the well-known relation $R_{ee} = l_0\sqrt{n_0 C_\infty}$, where C_∞ is the Flory characteristic ratio,[45] n_0 and l_0 are the number and length of monomer units in the considered chain respectively (see Table 1). The minimal inner thickness of the studied multinanolayer films is about 3 times higher than R_{ee} for all the different polymers. So, following Wang *et al.*[58] we assume that M_e is constant in the range of thicknesses studied.

3.1 T_g of multinanolayer films

From DMA it is possible to extract the glass transition temperature for multinanolayer films. Fig. 2a displays the normalized glass transition temperature (*i.e.* T_g obtained from the films tested by DMA divided by T_g of the neat polymer) for PS, PMMA, PC and SAN against the individual layer thickness h. The color bar indicates the number of total layers in the films. For both polymer pairs, we observe that the T_g is constant in the range of thicknesses studied, and close to the bulk value. The slightly larger deviation from the bulk value for the PC/SAN pair compared to the PS/PMMA pair is a signature of their better compatibility.[46] Note that in PS/PMMA multinanolayer films, only one T_g was observed, due to the closeness of the T_g values for PS and PMMA (see Table 1). This leads to a simplified version of Bay's model for the multinanolayer films:

$$E_m = \alpha(T - T_g) + \beta \exp\left(\frac{-2}{\langle M_w/M_e\rangle}\right) \qquad (4)$$

Then, DMA is used to examine the validity of eqn (4) for the PS/PMMA multinanolayer films. To do so, the dynamic Young modulus E^* is plotted in Fig. 2b against $T - T_{g_{bulk}}$. As expected, when the temperature gets closer to the T_g, there is a sharp decrease of E^* for all samples. Moreover, as the changes are small and hardly quantifiable in DMA, the effect of the total number of layers (and of the layer thickness) on the variation of E^* with temperature will be neglected in a first approach. Looking at the evolution of the modulus sufficiently far from T_g (inset in Fig. 2b), a linear relationship as proposed in eqn (4) captures correctly the trend and provides values for α and β, $\alpha_{DMA} \approx -13.5$ MPa $^\circ C^{-1}$ and $\beta_{DMA} \approx 2.1$ GPa respectively (orange dashed line in inset in Fig. 2b). It should be noted that these values are in reasonable agreement with those that can be extracted from Bay's work[10] (see Table S1 in ESI†): approximating the modulus with $\sigma_{max}/\epsilon_{\sigma_{max}}$ for 150 nm PS films with molar masses similar to those of this study (number average molecular weights of 127 kg mol^{-1} and 98 kg mol^{-1}) leads to $\alpha_B \sim -18$ MPa $^\circ C^{-1}$ and $\beta_B \sim 1.8$ GPa, which further validates the extension of Bay's stress model to the modulus. Fig. S4 (in ESI†) shows a similar behavior for the PC/SAN multinanolayer films.

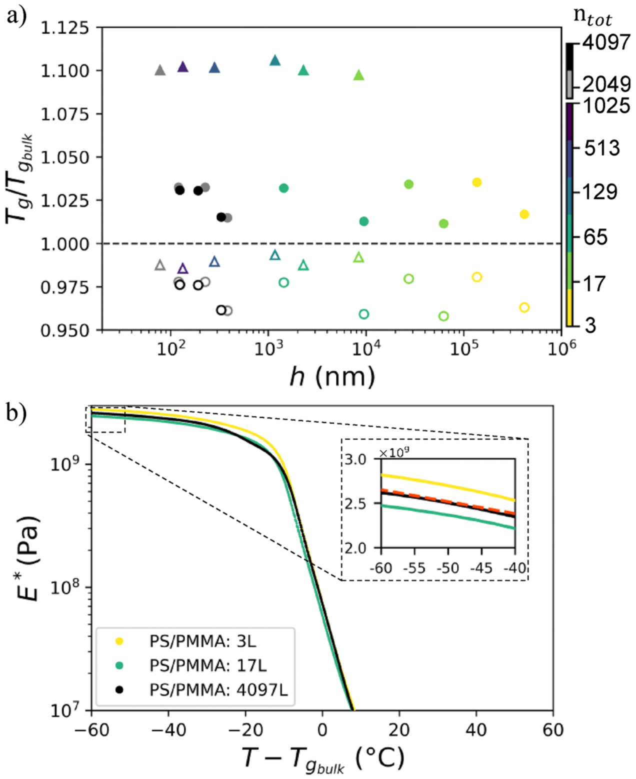

Fig. 2 Dynamic mechanical analysis of multinanolayer polymer films with the colour representing the total number of layers in the samples. (a) Dimensionless glass transition temperature as a function of the internal thickness h. Circles represent the experimental T_g of PS/PMMA films divided by the bulk T_g of PMMA (●, filled circle) and PS (○, open circle). Triangles represent the experimental T_g of SAN in PC/SAN films divided by the bulk T_g of SAN (▲, filled triangle) and the experimental T_g of PC in PC/SAN films divided by the bulk T_g of PC (Δ, open triangle). (b) Dynamic Young's modulus as a function of $T - T_g$ for different PS/PMMA films. The inset shows the temperatures close to RT in linear scale. Orange dashed curve is a linear fit, averaging the experimental data, leading to (α_{DMA}, β_{DMA}).

3.2 Young modulus from three-point bending test

Young's modulus of different multinanolayer films and for the neat polymers is obtained from the three-point bending tests performed at RT. For PS and PMMA neat films, average Young moduli of 3.1 and 3.4 GPa are obtained respectively, in agreement with literature data[57] and similar to E^* from the DMA experiments (though about 20% higher). First, Young's modulus is measured for samples cut orthogonal or parallel to the extrusion flow. Fig. S2b in ESI† shows that both samples yield close values. In consequence, only samples cut parallel to the extrusion flow are discussed in the following.

Fig. 3a shows, for the three different polymer pairs, the evolution of the Young modulus normalized by E_{film} (rule of mixtures), as a function of the layer thickness of the inner polymer. To analyze the trends, individual data are collected into five groups with different thicknesses, ranging from ∼100 nm to ∼100 μm. Tukey's honest significant difference (HSD) test at the 5% significance level is then conducted to compare the different datasets (see details in Tables S3 and S4 in ESI†).[59] It is seen that

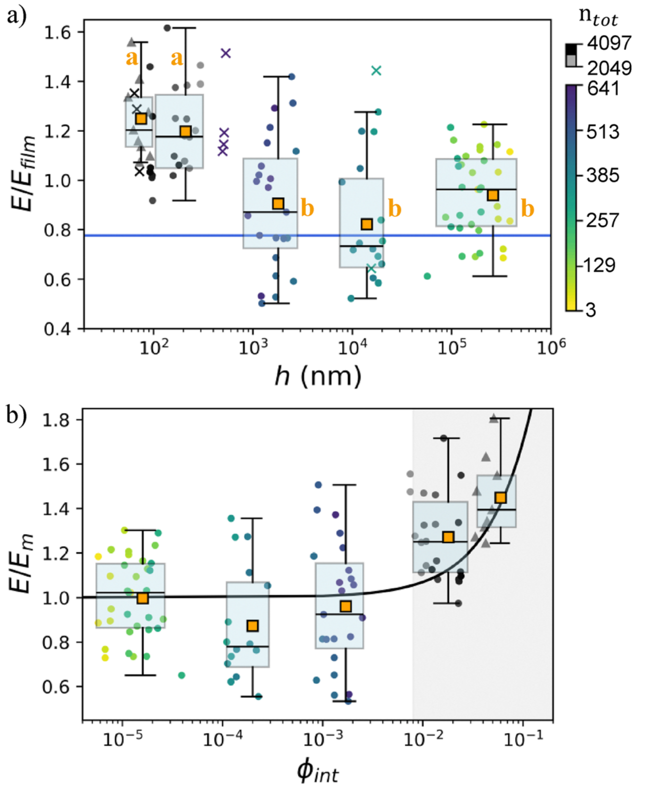

Fig. 3 Three-point bending tests at room temperature for multinanolayer polymer films, with (●) PS/PMMA, (▲) PC/SAN, (×) (PE/PEgMA/PA). (a) Box plot of the normalized Young modulus (with E_{film} from the rule of mixtures) as a function of the layer thickness h. Blue line is obtained from eqn (4) for PS/PMMA. (b) Box plot of the normalized Young modulus, here with E_m from eqn (4), as a function of the volume fraction of the interphase ϕ_{int} from eqn (5). Black curve represents the model of eqn (6) which takes in consideration the presence of the interphase. For both figures, the box indicates the upper and lower quartiles of the experimental values. The whiskers are determined by the minimum and maximum experimental value. The horizontal line inside the box represents the median, and the orange square represents the mean. Dataset with different letters (a or b) are significantly different according to the Tukey-test at the 5% significance level (see Tables S3 and S4 in ESI†).

for $h < 1$ μm (thin film regime) there is a statistically significant increase in the measured modulus for the three different types of multinanolayer films, while the values for $h > 1$ μm (bulk regime) can be considered constant.

E_m/E_{film} of PS/PMMA (with E_m obtained from eqn (4) with α_{DMA} and β_{DMA} values) is shown as a blue line. Both the rule of mixtures and Bay's adapted model predict a modulus that is independent of the layer thickness. They also give similar values for the modulus, in good agreement with the experiments. While the rule marginally overestimates the bulk modulus, Bay's adapted model underestimates it, which is simply due to the fact that the DMA measured modulus is slightly lower than the bending one.

3.3 Role of the interphase

To account for this increase in modulus at small layer thicknesses, we will consider in the following the absence of free surfaces in our multinanolayer films and their replacement by interphases, the role of which we are going to examine. The volume fraction of the interphase can be expressed as:

$$\phi_{int}(a,h) = (n_{tot}-1)\frac{a}{H} = \frac{n_{tot}-1}{n}\phi\frac{a}{h} \approx 2\phi\frac{a}{h} \tag{5}$$

If the layer thickness is below 100 nm, ϕ_{int} can reach values in the 1–10% range and is not negligible anymore. The increase in Young's modulus as the layer thickness decreases may then be related to this increase in ϕ_{int}. To illustrate this, the modulus, this time normalized by E_m is plotted as a function of the volume fraction of the interphase in Fig. 3b. When ϕ_{int} increases (h decreases), Young's modulus increases, with a deviation that becomes significant when $\phi_{int} \gtrsim 1\%$ (gray area in Fig. 3b). To focus specifically on the increase in modulus at high volume fractions, and since the HSD test determined that the modulus could be considered constant at low volume fractions, the value of β is adjusted to the bending-test modulus, in order to have $E/E_m = 1$ in the bulk regime. This choice is also motivated by the relatively large uncertainty on β measurements, as shown in Bay *et al.*[10] A value of *i.e.* $\beta_{bending} \approx 2.8$ GPa is obtained, consistent with the values obtained in Tables S1 and S2 in ESI.† As a first approach, the effect of the interphase volume fraction can be taken into account using a linear regression, with a slope that may be termed the "Young modulus of the interphase" E_{int}. For the glassy PS/PMMA system, $E_{int_{PS/PMMA}} \approx 25$ GPa. This contribution of the interphase is then added to eqn (4), leading to a new empirical version of Bay's model adapted to multinanolayer films:

$$\begin{aligned} E_{multi}(T_g,h) &= E_m(T_g) + C_{int}(h) \\ &= \alpha(T-T_g) + \beta\exp\left(\frac{-2}{\langle M_w/M_e\rangle}\right) + 2\phi\frac{a}{h}E_{int}, \end{aligned} \tag{6}$$

where $C_{int}(h)$ represents the contribution of the interphase for a given multinanolayer film (black line in Fig. 3b and 4).

3.4 Freestanding, supported and multinanolayer films

Now, it shall be interesting to compare more directly the experimental results and modeling for multinanolayer films (with no free surfaces) with results from the literature on ultra-thin films having one or two free surfaces (Fig. 1). Fig. 4 shows the experimental Young modulus normalized by the bulk value for PS (green squares) ultra-thin films with different molecular weights and two (empty symbols) or one (full symbols) free surfaces. The box plots are the experimental results for the multinanolayer films of the present study (in the case of the multinanolayers, the modulus has been normalized by E_{film}). The green curves are the corresponding fits using eqn (3) for each experimental data from the literature (used parameters are presented in Table S2 in ESI†), and the black curve is from the modified model presented in eqn (6). We observe that, although Bay's model captures adequately the decrease of modulus with decreasing thickness in the case of ultra-thin films, the modified version proposed in this study describes

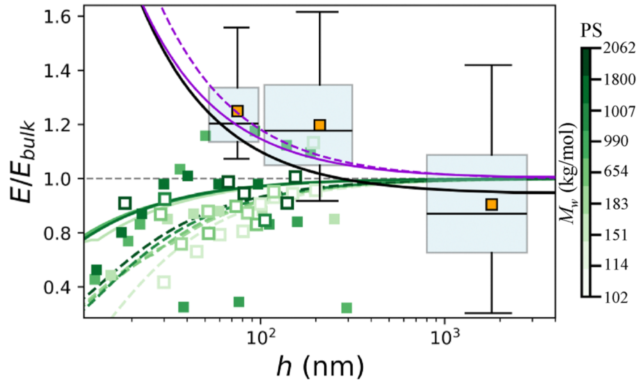

Fig. 4 Young's modulus as a function of thickness, for polymer films with different number of free surfaces. Boxes are taken from this study, solid black line represents the model proposed in eqn (6) for PS/PMMA. Filled and empty green squares are for supported and free-standing PS thin films respectively. The different shades are for different molar masses[11,12,26,60–62] (see scale bar on the right). Solid and dashed green lines are the best fits from eqn (3) for supported and freestanding PS ultra-thin films respectively (see Table S2 in ESI†). Purple solid and dashed lines represent the modified mixing rule model including the interphase contribution ($E_{\text{film w/int}}$) for PS/PMMA and PC/SAN films respectively (see eqn (S3) in ESI†).

accurately the trend of the experimental data for multinanolayer films. This showcases the role of the number of free surfaces in the mechanical properties of ultra-thin polymer films. It shall be noted that an approach based on a modified mixing rule model including an interphase contribution (eqn (S3) in ESI†), represented by solid and dashed purple lines in Fig. 4 for PS/PMMA and PC/SAN respectively, also captures adequately the trend, while yielding similar values for the interphase moduli, for PS/PMMA $E_{\text{int}_{\text{PS/PMMA}}} \approx 26$ GPa, but for PC/SAN as well, with $E_{\text{int}_{\text{PC/SAN}}} \approx 27$ GPa (see Fig. S5 in ESI†).

However, films made with PC/SAN have a theoretical interphase thickness about twice the one of PS/PMMA. An interesting observation that can be made from the comparison of these two polymer pairs is that the global increase of films' modulus with decreasing layer thickness seems independent from the presence of entanglements at the interfaces. For PS and PMMA, the mean entanglement spacing (obtained from the molecular weight between entanglements listed for example in Fetters *et al.*[45]) is about 8 nm, much larger than $a_{\text{PS/PMMA}}$, while it is close to 4 nm for PC and SAN, this time smaller than $a_{\text{PC/SAN}}$. Hence, contrary to other properties such as interfacial adhesion[39,40] which heavily depends on the presence of entanglements, it seems a unique value for "Young's modulus of the interphase" can be defined, $E_{\text{int}} \approx 25$ GPa, not related to the compatibility of the glassy polymers constituting the multinanolayer films. Another interesting observation is that PE/PA6 multinanolayer films ((×) symbols in Fig. 3a) show similar trends as the PS/PMMA and PC/SAN film, despite being semi-crystalline materials. This, along with the fact that E_{int} is constant, reinforces the hypothesis that the mechanical behavior of these films is mostly governed by the interphases rather than by the nature of the polymers involved.

As a final cautious note, it is worth noting that this discussion is based on a theoretical estimate of the interphase thickness assuming random coil conformation, while the polymer chains might not be at equilibrium due to the coextrusion process, especially the drawing and cooling stages. To the best of our knowledge, there are no direct means to measure the actual interphase thickness in such films. However, two studies linked macroscopic properties (oxygen permeability[46] and extensional viscosity[34]) to interfacial thickness. In these works, models using the equilibrium theoretical value were used to capture quantitatively the experimentally measured film properties, suggesting that it can be reasonably used as a first approach. Still, it is plausible that chains are actually stretched in the extrusion direction, which should create a thinner interphase than theoretically predicted. This, in turn, would lead to a higher value of the interphase modulus, and possibly different values for polymer pairs being more or less far away from equilibrium due to processing conditions.

4 Conclusions

Young's modulus of multinanolayer coextrusion films made of different polymer pairs has been measured by means of DMA and three-point bending tests. Such systems are of interest as the results show that in bending mode, the films with higher number of layers and smaller layer thicknesses display a higher modulus for every polymer pair studied, up to about 30%. In the literature, previous work has evidenced a decrease in Young's modulus of free-standing as well as supported ultra-thin films with decreasing thicknesses.[11,12,25,26,60–62] Put together, these results are not contradictory but rather confirm the influence of free surfaces in the physical and mechanical properties of thin polymer layers. Contrary to freestanding or supported ultra-thin films, multinanolayer films have no free surfaces. More precisely, they display thousands of polymer–polymer interfaces with (nanometric) thicknesses that are related to the polymers' compatibility, or in other words to the magnitude of the thermodynamic Flory interaction parameter. This absence of free surfaces is also consistent with constant T_g values (independent of the layer thicknesses) measured in multinanolayer films. A model is proposed that attributes the increase in Young's modulus to an increase in the volume fraction of the interphase, building on an approach previously used in the molten state with viscosity.[34,63] From this hypothesis, an interphase modulus is obtained, with a value of 25 GPa, about 10 times higher than the typical modulus value of a glassy polymer. An interesting result is that this value does not seem to depend on the presence of entanglements at the interface, as it is constant whether the polymer pair is incompatible (PS/PMMA) or compatible (PC/SAN), and further confirmed on a compatibilized (*i.e.* having a copolymer at the interface) system (PE/PA6). This differs from the quantitative relation established between entanglements and interfacial adhesion between polymer layers.

To explore in more details the reinforcing mechanisms of the interphases in these laminated structures, large deformation studies at low (puncture resistance) or large strain rates (impact) will be considered next. To further confirm the high interphase modulus independent of the polymer pair suggested from this macroscopic study, a direct and quantitative measurement using AFM coupled with nanoscale DMA can be envisioned.

Author contributions

Alvaro A. Grandi: conceptualization, methodology, validation, formal analysis, investigation, data curation, writing – original draft, writing – review & editing and visualization. Alain Guinault: conceptualization, methodology, resources and writing – review & editing. Jorge Peixinho: conceptualization, methodology, resources and writing – review & editing. Cyrille Sollogoub: conceptualization, methodology, resources and writing – review & editing. Arnaud Antkowiak: conceptualization, methodology and writing – review & editing. Sébastien Neukirch: conceptualization, methodology, writing – review & editing, supervision, project administration and funding acquisition. Guillaume Miquelard-Garnier: conceptualization, methodology, validation, resources, writing – original draft, writing – review & editing, supervision, project administration and funding acquisition.

Data availability

Data for this article, including experimental data, python scripts for data post-processing and plotting are available at Figshare at **https://doi.org/10.6084/m9.figshare.28742678**.

Conflicts of interest

There are no conflicts to declare.

Acknowledgements

A. Dmochowska, X. Mackré and Q. Beuguel are acknowledged for the fabrication of the multilayer films used in this study. J.-B. Marijon helped in setting up the bending test and E. Desarro to run some of the mechanical tests. F. Daghia is acknowledged for fruitful discussions and helpful experimental suggestions. Finally, S. Neukirch and G. Miquelard-Garnier would like to thank DIM MaTerRE for funding the post-doctoral fellowship of A. A. Grandi through the project INTIMAL. We would like to thank both reviewers for their careful reading of the manuscript and insightful comments.

References

1 S. A. Sukhishvili and S. Granick, *J. Am. Chem. Soc.*, 2000, **122**, 9550–9551.

2 J. Xu, S. Wang, G.-J. N. Wang, C. Zhu, S. Luo, L. Jin, X. Gu, S. Chen, V. R. Feig, J. W. F. To, S. Rondeau-Gagné, J. Park, B. C. Schroeder, C. Lu, J. Y. O. Oh, Y. Wang, Y.-H. Kim, H. Yan, R. Sinclair, D. Zhou, G. Xue, B. Murmann, C. Linder, W. Cai, J. B.-H. Tok, J. W. Chung and Z. B. Bao, *Science*, 2017, **355**, 59–64.

3 M. A. Priolo, D. Gamboa, K. M. Holder and J. C. Grunlan, *Nano Lett.*, 2010, **10**, 4970–4974.

4 J. Yu, K. Ruengkajorn, D.-G. Crivoi, C. Chen, J.-C. Buffet and D. O'Hare, *Nat. Commun.*, 2019, **10**, 2398.

5 J. L. Keddie, R. A. L. Jones and R. A. Cory, *EPL*, 1994, **27**, 59–64.

6 T. R. Böhme and J. J. De Pablo, *J. Chem. Phys.*, 2002, **116**, 9939–9951.

7 J. A. Forrest and K. Dalnoki-Veress, *Adv. Colloid Interface Sci.*, 2001, **94**, 167–195.

8 G. Vignaud, M. S. Chebil, J. Bal, N. Delorme, T. Beuvier, Y. Grohens and A. Gibaud, *Langmuir*, 2014, **30**, 11599–11608.

9 Z. Yang, Y. Fujii, F. K. Lee, C.-H. Lam and O. K. C. Tsui, *Science*, 2010, **328**, 1676–1679.

10 R. K. Bay, T. Zhang, S. Shimomura, M. Ilton, K. Tanaka, R. A. Riggleman and A. J. Crosby, *Macromolecules*, 2022, **55**, 8505–8513.

11 J. H. Lee, J. Y. Chung and C. M. Stafford, *ACS Macro Lett.*, 2012, **1**, 122–126.

12 C. M. Stafford, B. D. Vogt, C. Harrison, D. Julthongpiput and R. Huang, *Macromolecules*, 2006, **39**, 5095–5099.

13 J. M. Torres, C. M. Stafford and B. D. Vogt, *ACS Nano*, 2009, **3**, 2677–2685.

14 M. Tress, M. Erber, E. U. Mapesa, H. Huth, J. Müller, A. Serghei, C. Schick, K.-J. Eichhorn, B. Voit and F. Kremer, *Macromolecules*, 2010, **43**, 9937–9944.

15 H. Zhao, Z. Li, Y. Wang, Q.-A. Hong, W. Xia, Y.-C. Chiu and X. Gu, *Macromolecules*, 2024, **57**, 9121–9134.

16 O. Bäumchen, J. D. McGraw, J. A. Forrest and K. Dalnoki-Veress, *Phys. Rev. Lett.*, 2012, **109**, 1–5.

17 C. Zhang, Y. Guo and R. D. Priestley, *Macromolecules*, 2011, **44**, 4001–4006.

18 Y. Chai, T. Salez, J. D. McGraw, M. Benzaquen, K. Dalnoki-Veress, E. Raphaël and J. Forrest, *Science*, 2014, **343**, 994–999.

19 H. Yuan, J. Yan, P. Gao, S. K. Kumar and O. K. C. Tsui, *Sci. Adv.*, 2022, **8**, eabq5295.

20 R. P. White, C. C. Price and J. E. Lipson, *Macromolecules*, 2015, **48**, 4132–4141.

21 K.-I. Jo, Y. Oh, B. J. Sung, T.-H. Kim, M. S. Um, W. J. Choi, J. Bang, G. Yuan, S. K. Satija and J. Koo, *ACS Macro Lett.*, 2020, **9**, 210–215.

22 R. R. Baglay and C. B. Roth, *J. Chem. Phys.*, 2017, **146**, 203307.

23 J. Lee, S. Lee, K. Lee, H. Joung, S. K. Choi, M. Kim, J. Yang and K. Paeng, *J. Chem. Phys.*, 2024, **160**, 124902.

24 N. A. Garcìa and J.-L. Barrat, *Macromolecules*, 2018, **51**, 9850–9860.

25 R. K. Bay, S. Shimomura, Y. Liu, M. Ilton and A. J. Crosby, *Macromolecules*, 2018, **51**, 3647–3653.

26 L. A. Galuska, E. S. Muckley, Z. Cao, D. F. Ehlenberg, Z. Qian, S. Zhang, S. Rondeau-Gagné, M. D. Phan, J. F. Ankner, I. N. Ivanov and G. Xiaodan, *Nat. Commun.*, 2021, **12**, 2347.

27 A. G. Mikos and N. A. Peppas, *J. Chem. Phys.*, 1988, **88**, 1337–1342.

28 A. Bironeau, T. Salez, G. Miquelard-Garnier and C. Sollogoub, *Macromolecules*, 2017, **50**, 4064–4073.

29 Z. Li, A. Olah and E. Baer, *Prog. Polym. Sci.*, 2020, **102**, 101210.

30 D. Langhe and M. Ponting, *Manufacturing and novel applications of multilayer polymer films*, William Andrew, 2016.

31 E. Baer and L. Zhu, *Macromolecules*, 2017, **50**, 2239–2256.

32 H. Wang, J. K. Keum, A. Hiltner, E. Baer, B. Freeman, A. Rozanski and A. Galeski, *Science*, 2009, **323**, 757–760.

33 Q. Beuguel, A. Guinault, L. Léger, F. Restagno, C. Sollogoub and G. Miquelard-Garnier, *ACS Macro Lett.*, 2019, **8**, 1309–1315.

34 A. Dmochowska, J. Peixinho, C. Sollogoub and G. Miquelard-Garnier, *Macromolecules*, 2023, **56**, 6222–6231.

35 G. Ma, S. Zhang, L. A. Galuska and X. Gu, *J. Polym. Sci.*, 2024, **62**, 3839–3847.

36 Y. Zhu, A. Bironeau, F. Restagno, C. Sollogoub and G. Miquelard-Garnier, *Polymer*, 2016, **90**, 156–164.

37 M. S. Chebil, J. D. McGraw, T. Salez, C. Sollogoub and G. Miquelard-Garnier, *Soft Matter*, 2018, **14**, 6256–6263.

38 C. Creton, E. J. Kramer, C. Y. Hui and H. R. Brown, *Macromolecules*, 1992, **25**, 3075–3088.

39 H. R. Brown, *Macromolecules*, 2001, **34**, 3720–3724.

40 C. Creton, E. Kramer, H. Brown and C. Hui, *Adhesion and Fracture of Interfaces Between Immiscible Polymers: from the Molecular to the Continuum Scal*, Springer, Berlin, Heidelberg, 2002, pp. 53–136.

41 A. Bironeau, PhD thesis, HESAM, Paris, 2016.

42 S. F. Nassar, S. Domenek, A. Guinault, G. Stoclet, N. Delpouve and C. Sollogoub, *Macromolecules*, 2018, **51**, 128–136.

43 J.-S. Montana, S. Roland, E. Richaud and G. Miquelard-Garnier, *Polymer*, 2018, **136**, 27–36.

44 A. Bironeau, J. Dirrenberger, C. Sollogoub, G. Miquelard-Garnier and S. Roland, *J. Microsc.*, 2016, **264**, 48–58.

45 L. Fetters, D. Lohse, D. Richter, T. Witten and A. Zirkel, *Macromolecules*, 1994, **27**, 4639–4647.

46 R. Y. Liu, T. E. Bernal-Lara, A. Hiltner and E. Baer, *Macromolecules*, 2005, **38**, 4819–4827.

47 X. Mackré, PhD thesis, HESAM, Paris, 2023.

48 A. Dmochowska, J. Peixinho, C. Sollogoub and G. Miquelard-Garnier, *Rheol. Acta*, 2025, **64**, 7–19.

49 Q. Beuguel, A. Guinault, F. Chinesta, C. Sollogoub and G. Miquelard-Garnier, *J. Rheol.*, 2020, **64**, 981–989.

50 E. Helfand and Y. Tagami, *J. Chem. Phys.*, 1972, **56**, 3592–3601.

51 P. A. Russell, T. P. Hjelm Jr and R. P. Seeger, *Macromolecules*, 1990, **23**, 890–893.

52 G. Miquelard-Garnier and S. Roland, *Eur. Polym. J.*, 2016, **84**, 111–124.

53 S. Poincloux, T. Chen, B. Audoly and P. M. Reis, *Phys. Rev. Lett.*, 2021, **126**, 218004.

54 S. Timoshenko and J. M. Gere, *Theory of Elastic Stability*, McGraw-Hill international editions, 2nd edn, 1961.

55 J. M. Gere and B. J. Goodno, *Mechanics of Materials*, Cengage Learning, 2011.

56 D. R. Askeland, *The Science and Engineering of Materials*, Springer, Boston, MA, 1996.

57 M. F. Ashby, *Material Selection in Mechanical Design*, Elsevier Ltd., Burlington, MA, USA, 2011.

58 F. Wang, Z. Jiang, X. Lin, C. Zhang, K. Tanaka, B. Zuo, W. Zhang and X. Wang, *Macromolecules*, 2021, **54**, 3735–3743.

59 J. W. Tukey, *Biometrics*, 1949, **5**, 99–114.

60 R. K. Bay and A. J. Crosby, *ACS Macro Lett.*, 2019, **8**, 1080–1085.

61 D. Maillard, S. K. Kumar, B. Fragneaud, J. W. Kysar, A. Rungta, B. C. Benicewicz, H. Deng, L. C. Brinson and J. F. Douglas, *Nano Lett.*, 2012, **12**, 3909–3914.

62 J. M. Torres, C. M. Stafford and B. D. Vogt, *Polymer*, 2010, **51**, 4211–4217.

63 A. M. Jordan, B. Lee, K. Kim, E. Ludtke, O. Lhost, S. A. Jaffer, F. S. Bates and C. W. Macosko, *J. Rheol.*, 2019, **63**, 751–761.